Tailoring the surface morphology of Ni at the nanometric scale by ultrashort laser pulses

Anthony Nakhoul, Claire Maurice, Nicolas Faure, Florence Garrelie, Florent Pigeon, Jean-Philippe Colombier

Tailoring the Surface Morphology of Ni at the Nanometric Scale by Ultrashort Laser Pulses

Anthony Nakhoul[1,2], Claire Maurice[2], Nicolas Faure[1], Florence Garrelie[1], Florent Pigeon[1] and Jean-Philippe Colombier[1*]

[1*]Univ Lyon, UJM-Saint-Etienne, CNRS, IOGS, Laboratoire Hubert Curien UMR5516, F-42023 St-Etienne, France.
[2]Univ Lyon, Mines Saint-Etienne, CNRS, Centre SMS, Laboratoire Georges Friedel, UMR5307, F-42023 St-Etienne, France.

*Corresponding author(s). E-mail(s): jean.philippe.colombier@univ-st-etienne.fr;
Contributing authors: anthony.nakhoul@univ-st-etienne.fr;

Abstract

Ultrafast-laser irradiated surfaces are self-organizing systems that form intricated micropatterns and nanopatterns. Different shapes of randomly and periodically dispersed nanostructures emerge from a homogenous metal surface, resulting in a remarkable display of dissipative structures. Under femtosecond laser irradiation with a controlled amount of energy, the formation of nanobreath-figure, nanocrosshatch, nanopeaks, nanohumps, nanobumps, nanocavities and nanolabyrinthine patterns are reported. The fabrication of these 2D different nanostructures may allow for novel surface functionalizations aimed at controlling mechanical, biological, optical, or chemical surface characteristics on a nanometric scale. We demonstrate that using crossed-polarized double laser pulses adds a new dimension to the nanostructuring process since the laser energy dose and multi-pulse feedback modify the energy gradient distribution, crossing key levels for surface self-organization regimes.

Keywords: ultrafast laser, morphology control, 2D nanopatterns, self-organization

1 Introduction

Ultrashort laser energy deposition generates local thermal stresses and transient phase transitions, changing material microstructures and topographies[1]. Polarization effect of light interaction with material surfaces creates anisotropic surface morphology, called laser-induced periodic surface structures (LIPSS) or ripples[2]. LIPSS are nanopatterns with periodicities approaching laser wavelength down to sub-100 nm[3]. These structures can alter wetting[4], tribological, and optical characteristics[5]. Laser-induced textures provide hydrophobic[6], antimicrobial[7], colored[8], and wear-resistant surfaces[9]. Multi-pulse irradiation below the ablation threshold amplifies and regulates their development. The initial laser pulse randomly alters the surface topography by forming roughness centers. All subsequent laser pulses impinge the surface continually, changing by preceding pulses and roughening from a quasi-flat surface to transiently increasing irregularities[10]. LIPSS may be created with varied periodic scales on an irradiated surface via radiative and non-radiative light coupling, which involves polarization effects on newly formed roughness centers[11]. Most sub-wavelength structures are orientated by laser polarization, generally spaced between 50-200 nm in the literature and a priori caused by local field amplification on the local roughness[12]. Literature calls them high spatial frequency LIPSS (HSFL)[13]. Light coupling is composed of scattered waves and nonradiative fields that emerge from nanoreliefs, causing near field exaltations. Strong electromagnetic field increases at surface flaws trigger local heat confinement, destabilizing the thin laser-induced melt layer. During sub-surface rarefaction, cavitation creates nanovoids and nanocavities at the surface[14]. During rarefaction wave acceleration of the molten surface, hydrothermal waves perpendicular to temperature gradients can initiate a Marangoni-convection instability, generating periodic surface patterns[15].

Recent investigations show that two orthogonal linear polarization states can eliminate polarization dependence. Controlling ultrafast laser pulse polarization, inter-pulse delay, and laser fluence creates unique 2D surface morphologies. Several studies focused on near-submicron 2D-LIPSS have revealed the appearance of rhombus, triangle and spherical structures on cobalt[16], while others have reported triangular and square nanostructures by using double linearly crossed polarized and counter-rotating circularly polarized pulses on stainless steel with a time-delays in the picosecond range [17].These periodic nanostructures were created by scanning the surface and have a periodicity close to the laser wavelength. However, none of these studies have reported such symmetry features at the nanoscale

Driven by near-field light enhancement, periodic patterns have reached ultimate sizes of tens of nanometers on a (001)-oriented Nickel surface. A self-organizing array of nanocavities with a diameter of 20 nm and a periodicity of 60 nm was developed by a new technique[18]. By delaying cross-polarized laser pulses, this technique overcomes the anisotropic polarization response of the surface, allowing for self-arranged nanoscale topography in advanced

technological areas[19].This work explores the creation of unrevealed nanopatterns morphologies controlled by different energy doses, all well below the diffraction limit. We address the laser irradiation settings and material circumstances suited to induce nanostructuring self-organization. Under ultrafast excitation, a homogenous metal surface forms disordered, nanobreathfigure, nanocrosshatch, nanopeaks, nanohumps, nanobumps, nanocavities and nanolabyrinthine patterns.

1.1 Experimental details

1.1.1 Material preparation

This work employed a mono-crystalline Ni (001) sample bar produced via directed solidification and cut using a wire saw. Experiments included mechanical and electrochemical polishing. Automatic polishing was conducted on "Buehler Automet 250" using coarse paper of P180, advancing sequentially to P320, P600, P1200 and P2400 followed by a 3 µm and 1 µm diamond and vibratory polishing on "Buehler Vibromet 2" with colloidal silica 0.05 µm prior to laser irradiations. After automated polishing on "Struers LectroPol-5," electropolishing was conducted at 25 V for 60 s. Both polishing methods provide samples with an arithmetical mean surface roughness (Ra) less than 5 nm.

1.1.2 Laser irradiation

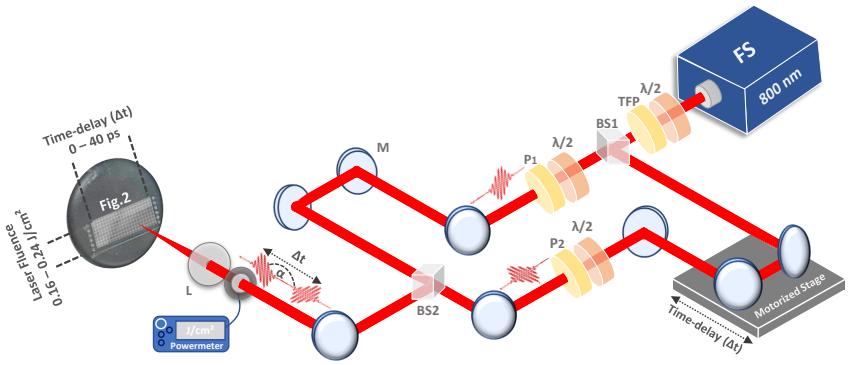

Fig. 1 Schematic illustration of femtosecond laser double pulse setup with a temporal control. FS represents the femtosecond laser, BS1 and BS2 refer to the beam splitters, $\lambda/2$ for the half-wave plate. TFP refers to the thin film polarizer, P for the polarizer, M for the mirror and L for the lens with a focal distance of 25 cm from the sample.

Coherent's Legend Elite Series Ti: Sapphire laser was utilized. It provides linearly polarized pulses with a minimum pulse duration around 40 fs. The ultrafast amplifier delivers a 1 kHz repetition rate, 3 W output power, and a

$\lambda = 800$ nm center wavelength. The ejection of the ultrashort pulse amplified by the pump laser is performed by a pulse picker.

Using a modified Mach–Zehnder interferometer, cross-polarized irradiation promotes self-organization by inducing isotropic energy deposition on the surface. The effect of crossed polarization is combined with an inter-pulse delay, which controls laser-induced structure creation. First, the incoming laser beam is divided in two by a non polarizing beam splitter with 50/50 ratio, represented by BS1 in Figure 1. These beams traverse two optical routes or arms before recombining at a second beam splitter BS2. A motorized stage controls the moveable arm's length, which leads to a temporal control between the first and second beam in the picosecond regime. Both arms energy can be controlled, as well as polarization, using $\lambda/2$ and polarizer.

At $\Delta t = 0$, temporal overlap occurs when the two optical pathways have the same length. The spatial overlap is verified on the autocollerator when the polarization angle is 0°. Each arm has a polarizer (P) to control the polarization angle between the two beams to achieve cross-polarization. The cross polarization is ensured by a polarizing beam splitter combined with a camera to assure the cross polarization with less time and more precision.

The light inside the Mach-Zehnder travels two different paths and recombines before being collimated by a 25 cm lens and irradiates a sample at normal incidence. The Gaussian profile at $(1/e^2)$ has a spot size of $2\omega_0 \approx 60$ µm, where ω_0 is the beam waist. The size of the laser spot is always measured before irradiation by the D^2 method[20]. A thin-film polarizer (TFP) which separate s and p polarization coupled with a $\lambda/2$ allows us to control the energy of pulses measured by a powermeter just before the Lens (L).

1.1.3 Characterization

Surface topography was observed using "JEOL" scanning electron microscopy (SEM) equipped with a field emission gun. Different magnitudes of pictures were captured at 3 kV using an Everhart–Thornley detector (ETD). For 2D and 3D characterization, "Bruker Dimension ICON" atomic force microscopy (AFM) was utilized. Images were captured using the AIR imaging mode with a silicon tip on a nitride lever and a resolution of about 1 nm for visualizing the surface topography of a material. Using the NanoScope Analysis program, topological analyses and roughness calculations were conducted.

Transmission electron microscopy was used to examine the microstructure of the cross-sectional lamella. High-resolution transmission electron microscopy (HR-STEM) was performed using a JEOL NEOARM microscope equipped with a spherical aberration corrector, operating at 200 kV with STEM-ADF. TEM lamella preparation was accomplished utilizing a FIB/SEM workstation (NVision 40; Carl Zeiss Microscopy GmbH) in conjunction with a SIINT zeta FIB column and a Gemini I column. The NVision 40 platform has a SIINT Gas Injection System with many nozzles (GIS). To achieve the final TEM lamella, cautious milling and low kV ion polishing were used (thickness around 100

nm). During preparation, precautions were made to reduce the curtain effect and surface implantation.

2 Results and discussions

Several organization regimes are presented in Figure 2 controlled by laser fluence and time-delay (Δt) between the two cross-polarized pulses at a fixed number of double-pulses sequences of 25 and pulse duration of $\approx$ 100 fs. A total of eight different organizations are observed. In Figure 2, the chaotic regime is presented in dark blue color, it is obtained at low $\Delta t \leq$14 ps and laser fluence between 0.19 and 0.24 J/cm^2.

The nanobreath-figure are observed in a smaller region where $\Delta t \approx 0$ ps and for a laser fluence between 0.20 and 0.22 J/cm^2. These nanopatterns are identified for the first time on Nickel. They have an unorganized cavity shape with dimensions at the nanoscale[21][22]. Nanocrosshatch are also observed at a $\Delta t \approx 0$ ps but at lower laser fluence between 0.17 and 0.19 J/cm^2. In this regime, two diagonal nanostripes superposed perpendicularly to each other are observed.

At larger time-delay between $6 \leq \Delta t \leq 10$ ps, the nanocrossatch are being transformed to a high aspect ratio nanopeaks. They have a diameter of $\approx$ 20 nm and a height of $\approx$ 100 nm[23]. By increasing the time-delay, nanopeaks are being transformed to nanobumps with a lower aspect ratio, they almost have a same height compared to nanopeaks but with a larger diameter of $\approx$ 100 nm and less concentration. They are presented in the purple region in Figure 2.

The nanohumps are presented in red color, they are found at time delay $\geq$ 10 ps. They are small humps with a low aspect ratio and a height around 10 nm. The nanovoids or nanocavities are formed at higher energy above 0.19 J/cm^2 and they are presented in dark green color. Their size is increasing while increasing the laser fluence to reach homogeneous shapes and organizations at a laser fluence of 0.24 J/cm^2 and a time delay of 24 ps.

Furthermore, labyrinthine nanostructures are observed at high laser fluence between 0.22 and 0.24 J/cm^2 and a large time-delay between $28 \leq \Delta t \leq 30$ ps. The fascinating labyrinthine shape is formed at a laser fluence of 0.23 J/cm^2 and a time-delay of 30 ps.

The pseudo 3D scanning electron microscopy images in Figure 3 present the observed regimes in Figure 2 for the best laser conditions to obtain uniform patterns at the center of the impact. Chaotic nanostructures are observed at a laser fluence of 0.24 J/cm^2 and for $\Delta t \approx 2$ ps as presented in Figure 3a. These nanostructures are ordinarily observed at high fluence and low time-delay. They do not have any organization or order and they present a disordered rough surface in the swelling regime. Energetically, it is somehow acting similarly to a single pulse process, at a cumulated absorbed fluence higher than the single-pulse absorbed threshold since the small delay leads to a slight decrease of Ni reflectivity with electronic thermal excitation before the second pulse[24].

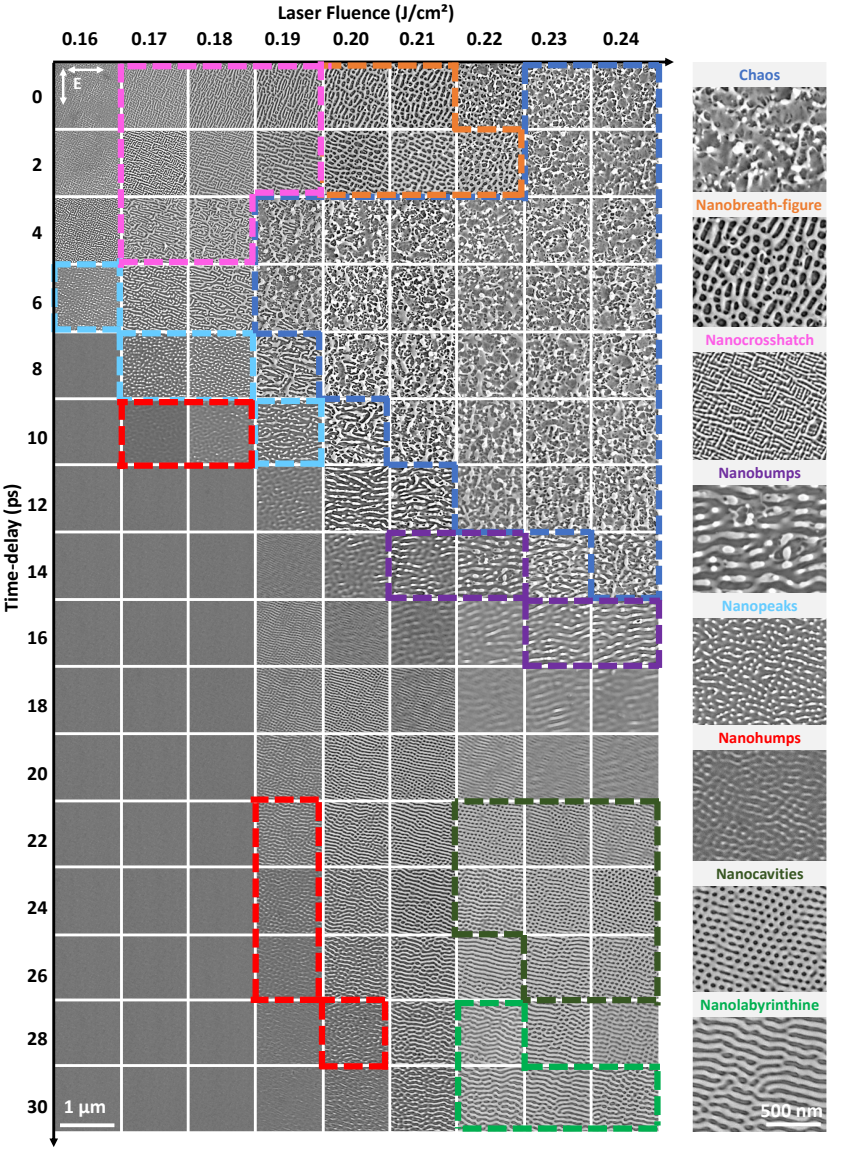

Fig. 2 a) Scanning electron microscopy of a Ni(001) crystal irradiated by 25 number of double-pulses sequences at an incident laser fluence range from 0.16 to 0.24 J/cm^2 with time-delay range from $0 \leq \Delta t \leq 30$ ps between the two crossed polarizations. The nanostructures domains are presented in different colored regions such as: dark blue for chaos, orange for nanobreath-figure, pink for nanocrosshatch, light blue for nanopeaks, red for nanohumps, purple for nanobumps, dark green for nanovoids and light blue for nanolabyrinthines. The laser polarization E is indicated by the white arrow.

Figure 3b presents the nanobreath-figure surface, their shape is similar to nanocavities but with less organisation and a larger size. They are presented

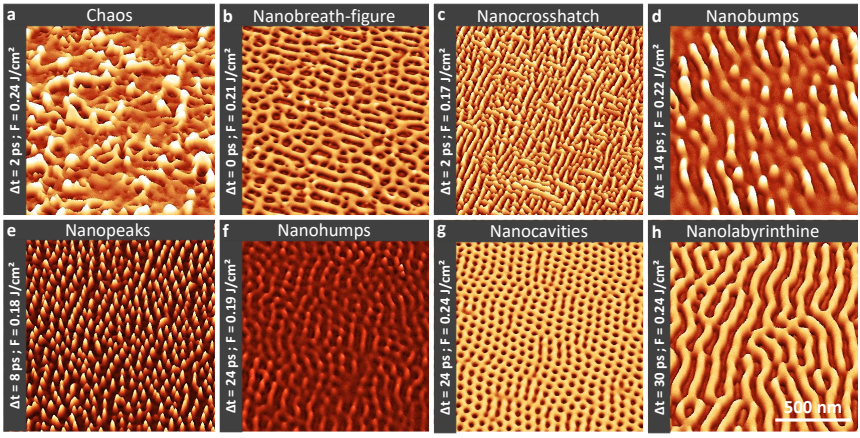

Fig. 3 a-h) Pseudo 3D scanning electron microscopy of nanostructures chaos (a), nanobreath-figure (b), nanocrosshatch (c), nanobumps (d), nanopeaks (e), nanohumps (f), nanocavities (g) and nanolabyrinthine (h).

for high uniformity condition at a laser fluence of 0.21 J/cm^2 and for $\Delta t \approx$ 0 ps. Nanocrosshatch topographies are presented in in Figure 3c, they look like crossed nanostripes nanostructures and they are formed at a laser fluence of 0.17 J/cm^2 and $\Delta t \approx 2$ ps. Nanobumps nanostructures are observed at a $\Delta t \approx 14$ ps and laser fluence of 0.22 J/cm^2 in Figure 3d. They are named as nanobumps corresponding to their lower aspect ratio and bumby surface. Figure 3e presents a forest of high aspect ratio nanostructures with a large concentration and great organization. They have a shape comparable to a karst peak, so they are named as "nanopeaks"[23]. They are formed at a laser fluence of 0.18 J/cm^2 and for $\Delta t \approx 8$ ps. However, nanohumps are also a periodic and organised nanostructures but they have a low aspect ratio compared to nanopeaks and very low height compared to nanobumps as shown in Figure 3f. They are optimally formed at a laser fluence condition at a laser fluence of 0.19 J/cm^2 and for $\Delta t \approx 24$ ps.

Hexagonal nanocavities or nanovoids patterns are observed for a time delay range between $22 \leq \Delta t \leq 24$ ps and a laser fluence between 0.22 and 0.24 J/cm^2. They are presented in Figure 3g in highest uniformity condition and best organization at 24 ps and 0.24 J/cm^2. Labyrinthine nanopatterns are observed at a higher time-delay range between $28 \leq \Delta t \leq 30$ ps and laser fluence between 0.22 and 0.24 J/cm^2. They are disordered spatial structures that show short-range order.

Figure 4 presents the 3D atomic force microscopy and transmission electron microscopy of the main nanostructures presented previously. The observed AFM images in Figure 4a shows the large nanobumps height, reaching up to $\approx$ 106 nm and the cross sectional view on Figure 4e presents the diameter of $\approx$ 100 nm. Figure 4b presents a forest of high aspect ratio nanopeaks, they have a height of $\approx$ 100 nm and a diameter of $\approx$ 20 nm as presented in Figure

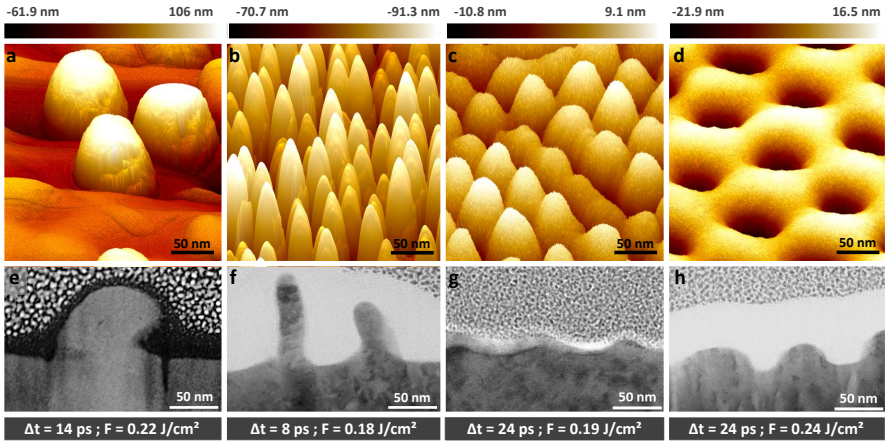

Fig. 4 3D atomic force microscopy of the nanobumps (a), nanopeaks (b), nanohumps (c) and nanocavities (d) presenting the nanostructures height and distribution. Transmission electron microscopy of the principles nanostructures presenting the cross sectional view of nanostructures.

4f. The nanohumps in Figure 4c shows the small height of ≈ 10 nm of these organised nanostructures and their diameter of ≈ 25 nm as shown in Figure 4g. Moreover, the nanocavities nanostructures in Figure 4d present hexagonal organisation with a depth of ≈ 20 nm and a diameter of ≈ 30 nm as presented in the cross sectional image. No ablation crater is observed by AFM and TEM even at the highest number of pulses and we remain in a regime of liquid layer formation without micrometric ablation. We are in the liquefaction/swelling regime.

The nonlinear mechanisms behind symmetry breaking and pattern selection in convective instabilities remain complex and still unresolved, yielding hardly predictable the transition conditions from a self-organization regime to another[25]. As a general picture these nanostructures are generated during the competition of the pressure gradient forces, mainly implying surface tension and cavitation process (through rarefaction) and the fast resolidification of the molten surface area. Thermo-convective instabilities may cause the fluid flow as a consequence of comparable transverse and longitudinal thermal gradients [15][26]. 2D symmetries are greatly favored by the consecutive use of two orthogonal electric field polarizations. The low fluence and pulse number conditions maintain the system near the melting threshold. Surface protrusions can then stem from fluctuations and grow at the nanometer scale fostering near-field light coupling. Specific laser conditions such as peak fluence, time delay, and number of double-pulse sequences have a crucial influence on thermally-driven convection features, affecting surface morphology and topography. In that respect, irradiation parameters determine emergence, growth and control of pattern development.

3 Conclusion

Several nanopatterns representing unique self-organization regimes were studied by femtosecond laser on nickel surfaces. An intense light energy exchange with a dissipative environment results in intricated 2D patterns of structures forming far from equilibrium. We demonstrate that a modest change in the amount and timeframe of energy delivery perturbs the system, leading to a transition from one stable self-organization regime to one with new features. The self-formation of nanobreath-figure, nanocrosshatch, nanopeaks, nanohumps, nanobumps, nanocavities and nanolabyrinthine patterns are reported. Irradiation conditions defined by peak fluence, time-delay, and the number of double-pulse sequences have a key role to select competing surface patterns by sequentially fostering emergence, growth, amplification, and regulation of pattern development. The degree of instability of such patterns is so high that the nanostructure shape organization can be altered by a few picoseconds delay change. These states are characteristic of attractors toward which the dynamical system tends to evolve in dissipative structures. The door is open to describe mathematically the nonlinear dynamics of laser-induced surfaces with models able to reproduce the variability of the patterns in the phase space and explore the origin of bifurcations.

Acknowledgments. This work was carried out thanks to the financial support of the Project ANR-17-EURE-0026 within the framework of the Programme Investissement d'Avenir.

4 Declarations

Conflict of Interests. The authors declare no confict of interest regarding the publication of this manuscript.

References

[1] Sedao, X., Maurice, C., Garrelie, F., Colombier, J.-P., Reynaud, S., Quey, R., Pigeon, F.: Influence of crystal orientation on the formation of femtosecond laser-induced periodic surface structures and lattice defects accumulation. Appl. Phys. Lett. **104**(17), 171605 (2014). https://doi.org/10.1063/1.4874626

[2] Varlamova, O., Martens, C., Ratzke, M., Reif, J.: Genesis of femtosecond-induced nanostructures on solid surfaces. Appl. Opt. **53**(31), 10–15 (2014). https://doi.org/10.1364/AO.53.000I10

[3] Bonse, J., Krüger, J., Höhm, S., Rosenfeld, A.: Femtosecond laser-induced periodic surface structures. J. Laser Appl. **24**(4), 042006 (2012). https://doi.org/10.2351/1.4712658

[4] Wu, Z., Yin, K., Wu, J., Zhu, Z., Duan, J.-A., He, J.: Recent advances in femtosecond laser-structured Janus membranes with asymmetric surface wettability. Nanoscale **13**(4), 2209–2226 (2021). https://doi.org/10.1039/D0NR06639G

[5] Bonse, J.: Quo Vadis LIPSS?—Recent and Future Trends on Laser-Induced Periodic Surface Structures. Nanomaterials **10**(10), 1950 (2020). https://doi.org/10.3390/nano10101950

[6] Zorba, V., Stratakis, E., Barberoglou, M., Spanakis, E., Tzanetakis, P., Anastasiadis, S.H., Fotakis, C.: Biomimetic Artificial Surfaces Quantitatively Reproduce the Water Repellency of a Lotus Leaf. Adv. Mater. **20**(21), 4049–4054 (2008). https://doi.org/10.1002/adma.200800651

[7] Elbourne, A., Crawford, R.J., Ivanova, E.P.: Nano-structured antimicrobial surfaces: From nature to synthetic analogues. J. Colloid Interface Sci. **508**, 603–616 (2017). https://doi.org/10.1016/j.jcis.2017.07.021

[8] Vorobyev, A.Y., Guo, C.: Colorizing metals with femtosecond laser pulses. Appl. Phys. Lett. **92**(4), 041914 (2008). https://doi.org/10.1063/1.2834902

[9] Bonse, J., Koter, R., Hartelt, M., Spaltmann, D., Pentzien, S., Höhm, S., Rosenfeld, A., Krüger, J.: Tribological performance of femtosecond laser-induced periodic surface structures on titanium and a high toughness bearing steel. Appl. Surf. Sci. **336**, 21–27 (2015). https://doi.org/10.1016/j.apsusc.2014.08.111

[10] Zhang, H., Colombier, J.-P., Li, C., Faure, N., Cheng, G., Stoian, R.: Coherence in ultrafast laser-induced periodic surface structures. Phys. Rev. B **92**(17), 174109 (2015). https://doi.org/10.1103/PhysRevB.92.174109

[11] Rudenko, A., Mauclair, C., Garrelie, F., Stoian, R., Colombier, J.P.: Light absorption by surface nanoholes and nanobumps. Appl. Surf. Sci. **470**, 228–233 (2019). https://doi.org/10.1016/j.apsusc.2018.11.111

[12] Rudenko, A., Colombier, J.-P., Höhm, S., Rosenfeld, A., Krüger, J., Bonse, J., Itina, T.E.: Spontaneous periodic ordering on the surface and in the bulk of dielectrics irradiated by ultrafast laser: a shared electromagnetic origin. Sci. Rep. **7**(12306), 1–14 (2017). https://doi.org/10.1038/s41598-017-12502-4

[13] Skolski, J.Z.P., Römer, G.R.B.E., Obona, J.V., Ocelik, V., Huis in 't Veld, A.J., De Hosson, J.Th.M.: Laser-induced periodic surface structures: Fingerprints of light localization. Phys. Rev. B **85**(7), 075320 (2012). https://doi.org/10.1103/PhysRevB.85.075320

[14] Sedao, X., Abou Saleh, A., Rudenko, A., Douillard, T., Esnouf, C., Reynaud, S., Maurice, C., Pigeon, F., Garrelie, F., Colombier, J.-P.: Self-Arranged Periodic Nanovoids by Ultrafast Laser-Induced Near-Field Enhancement. ACS Photonics **5**(4), 1418–1426 (2018). https://doi.org/10.1021/acsphotonics.7b01438

[15] Rudenko, A., Abou-Saleh, A., Pigeon, F., Mauclair, C., Garrelie, F., Stoian, R., Colombier, J.P.: High-frequency periodic patterns driven by non-radiative fields coupled with Marangoni convection instabilities on laser-excited metal surfaces. Acta Mater. **194**, 93–105 (2020). https://doi.org/10.1016/j.actamat.2020.04.058

[16] Jalil, S.A., Yang, J., ElKabbash, M., Cong, C., Guo, C.: Formation of controllable 1D and 2D periodic surface structures on cobalt by femtosecond double pulse laser irradiation. Appl. Phys. Lett. **115**(3), 031601 (2019). https://doi.org/10.1063/1.5103216

[17] Fraggelakis, F., Mincuzzi, G., Lopez, J., Manek-Hönninger, I., Kling, R.: Controlling 2D laser nano structuring over large area with double femtosecond pulses. Appl. Surf. Sci. **470**, 677–686 (2019). https://doi.org/10.1016/j.apsusc.2018.11.106

[18] Abou Saleh, A., Rudenko, A., Reynaud, S., Pigeon, F., Garrelie, F., Colombier, J.-P.: Sub-100 nm 2D nanopatterning on a large scale by ultrafast laser energy regulation. Nanoscale **12**(12), 6609–6616 (2020). https://doi.org/10.1039/C9NR09625F

[19] Nakhoul, A., Maurice, C., Agoyan, M., Rudenko, A., Garrelie, F., Pigeon, F., Colombier, J.-P.: Self-Organization Regimes Induced by Ultrafast Laser on Surfaces in the Tens of Nanometer Scales. Nanomaterials **11**(4), 1020 (2021). https://doi.org/10.3390/nano11041020

[20] Liu, J.M.: Simple technique for measurements of pulsed Gaussian-beam spot sizes. Opt. Lett. **7**(5), 196–198 (1982). https://doi.org/10.1364/OL.7.000196

[21] Guo, T., Han, K., Heng, L., Cao, M., Jiang, L.: Ordered porous structure hybrid films generated by breath figures for directional water penetration. RSC Adv. **5**(107), 88471–88476 (2015). https://doi.org/10.1039/C5RA13627J

[22] Zhang, A., Bai, H., Li, L.: Breath Figure: A Nature-Inspired Preparation Method for Ordered Porous Films. Chem. Rev. **115**(18), 9801–9868 (2015). https://doi.org/10.1021/acs.chemrev.5b00069

[23] Nakhoul, A., Rudenko, A., Maurice, C., Reynaud, S., Garrelie, F., Pigeon, F., Colombier, J.-P.: Boosted Spontaneous Formation of High-Aspect

Ratio Nanopeaks on Ultrafast Laser-Irradiated Ni Surface. Adv. Sci. **9**(21), 2200761 (2022). https://doi.org/10.1002/advs.202200761

[24] Bévillon, E., Stoian, R., Colombier, J.P.: Nonequilibrium optical properties of transition metals upon ultrafast electron heating. J. Phys.: Condens. Matter **30**(38), 385401 (2018). https://doi.org/10.1088/1361-648x/aad8e5

[25] Brandao, E., Colombier, J.-P., Duffner, S., Emonet, R., Garrelie, F., Habrard, A., Jacquenet, F., Nakhoul, A., Sebban, M.: Learning PDE to Model Self-Organization of Matter. Entropy **24**(8), 1096 (2022). https://doi.org/10.3390/e24081096

[26] Tsibidis, G.D., Fotakis, C., Stratakis, E.: From ripples to spikes: A hydrodynamical mechanism to interpret femtosecond laser-induced self-assembled structures. Phys. Rev. B **92**(4), 041405 (2015). https://doi.org/10.1103/PhysRevB.92.041405